Inorganic Chemistry

Article

pubs.acs.org/IC

Modeling the Magnetic Properties and Mössbauer Spectra of Multifunctional Magnetic Materials Obtained by Insertion of a Spin-Crossover Fe(III) Complex into Bimetallic Oxalate-Based Ferromagnets

S. M. Ostrovsky,[†] O. S. Reu,[†] A. V. Palii,[†] M. Clemente-León,[‡] E. Coronado,[‡] J. C. Waerenborgh,[§] and S. I. Klokishner*,[†]

[†]Institute of Applied Physics, Academy of Sciences of Moldova, Academy Street 5, Kishinev, MD-2028, Moldova

[‡]Instituto de Ciencia Molecular (ICMol), Universitat de Valencia, Catedrático José Beltrán 2 46980 Paterna, Spain

[§]IST/ITN, Instituto Superior Técnico, Universidade Técnica de Lisboa, CFMC-UL 2686-953 Sacavém, Portugal

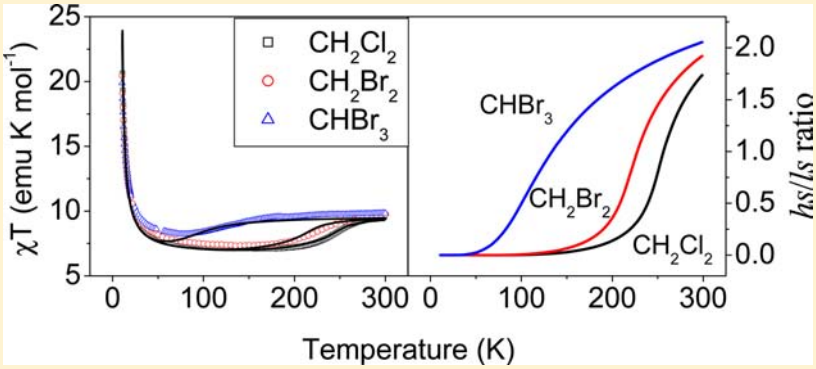

ABSTRACT: In this article, we present a theoretical microscopic approach to describe the magnetic and spectroscopic behavior of multifunctional hybrid materials which demonstrate spin crossover and ferromagnetic ordering. The low-spin to high-spin transition is considered as a cooperative phenomenon that is driven by the interaction of the electronic shells of the Fe ions with the full symmetric deformation of the local surrounding that is extended over the crystal lattice via the acoustic phonon field. The proposed model is applied to the analysis of the series $[Fe^{III}(sal_2\text{-trien})]$ $[Mn^{II}Cr^{III}(ox)_3]\cdot$solv, in short **1**·solv, where solv = CH_2Cl_2, CH_2Br_2, and $CHBr_3$.

1. INTRODUCTION

Octahedral transition metal complexes with d^4, d^5, d^6, and d^7 configurations can possess two different electronic ground states. These states are characterized by different orbital and spin multiplicities and are known as low-spin (ls) and high-spin (hs) states. More than 80 years ago, the temperature-induced spin-crossover transition between these states was discovered by Cambi et al. in a series of Fe^{III} tris-dithiocarbamate compounds.[1,2] Since then, numerous compounds of Fe^{II} ($3d^6$), Fe^{III} ($3d^5$), and Co^{II} ($3d^7$) have been reported to exhibit spin crossover both in the solid state and in solution (see review articles[3,4] and refs therein).

Spin-crossover compounds are of interest because they represent one of the best-known forms of inorganic electronic switches. Variation of the ground state in these compounds leads to both electronic (change in the occupation of the d-orbitals) and structural changes. Usually the ls ↔ hs transitions are gradual, but in some special cases, the conversion can become abrupt and accompanied by thermal hysteresis and bistability.[3,5−8] In processing of experimental data on spin-crossover systems, very often the semiempirical thermodynamic treatment is applied.[9−11] Another approach that is extensively used for the description of cooperativity in spin-crossover systems was suggested by Wajnflasz and Pick (WP) in the early seventies[12] and actually presents an Ising-like model, in which the ls and hs states are described by a fictitious spin $\sigma = -1$ and 1, respectively, and, along with a semiempirical ratio $g = g_{hs}/g_{ls}$ of the degeneracies g_{hs} and g_{ls} of the hs and ls states, a temperature-dependent effective gap is introduced. The WP model and its extensions called "Ising-like models" have been widely applied to the description of spin-crossover and related relaxation phenomena.[13−19]

The first microscopic approach to the problem of spin crossover was suggested by Kambara and then by Sasaki and Kambara.[20−22] In the framework of this approach the spin conversion was shown to be induced by the intermolecular spin coupling mediated by the lattice vibration modes and the lattice strain. For the first time in[23−25] the important feature of spin crossover compounds, i.e., the difference in the softness of the

Received: August 2, 2013
Published: November 13, 2013

medium between the spin crossover molecules and that inside the molecules was discussed. In refs 23−25, it was demonstrated that this model goes beyond the semiempirical thermodynamic[9−11] and WP approaches[12−19] and gives the possibility to take into account all relevant interactions (internal and external) and to write them down in the genuine basis of electronic states. Microscopic models of cooperative spin crossover in crystals containing Mn^{III} ions and cluster $\{[M^{III}(CN)_6]_2[M'^{II}(tmphen)_2]_3\}$ (M/M′ = Co/Fe, Fe/Fe) compounds based on the approach suggested in refs 23−26 have been presented in papers.[27,28] In refs 29 and 30, this approach has been generalized to the case of charge-transfer-induced spin transitions.

Recent efforts have led to the synthesis and characterization of new multifunctional molecular materials[31−35] with coexistence of ferromagnetism and spin-crossover. These materials represent salts formed by the insertion of spin-crossover iron(III) cation complexes into anionic coordination polymers based on homo- and bimetallic oxalate complexes. It has been shown in ref 32 that by changing the experimental conditions, two different oxalate networks with 2D and unusual achiral 3D structure can be obtained with the same templating cation, $[Fe(sal_2\text{-trien})]^+$. The 2D materials consist of honeycomb anionic layers formed by magnetic ions linked through oxalate ligands and cationic layers of spin crossover $[Fe^{III}(sal_2\text{-trien})]^+$ complexes intercalated between the 2D oxalate network. The magnetic properties and Mössbauer spectra of the 2D compound $[Fe^{III}(sal_2\text{-trien})][Mn^{II}Cr^{III}(ox)_3]\cdot CH_2Cl_2$[32] indicate that it undergoes a long-range ferromagnetic ordering at temperatures of a few Kelvin and a spin crossover of the intercalated iron complexes above 100 K. Such a type of compounds opens a way to design switching magnets in which the magnetic ordering of the oxalate network could be tuned, thus taking advantage of the changes in internal pressure induced by the spin-crossover phenomenon when applying external stimuli such as light or pressure. However, up to now the magnetic ordering and spin-crossover phenomena in the above-mentioned systems are not synchronized.[35] To solve this problem one needs deep understanding of the key mechanisms governing cooperativity in the two subsystems (spin-crossover and magnetic) and the interaction between them. With this aim in mind in the present paper we model three new compounds $[Fe^{III}(sal_2\text{-trien})][Mn^{II}Cr^{III}(ox)_3]\cdot CH_2Cl_2$,[32] $Fe^{III}(sal_2\text{-trien})][Mn^{II}Cr^{III}(ox)_3]\cdot CH_2Br_2$ and $[Fe^{III}(sal_2\text{-trien})][Mn^{II}Cr^{III}(ox)_3]\cdot CHBr_3$,[35b] in short **1**·solv, where solv = CH_2Cl_2, CH_2Br_2, and $CHBr_3$. The structure, magnetic properties and Mössbauer spectra of these compounds confirm spin crossover of Fe^{III} ions and ferromagnetic ordering in the $Mn^{II}Cr^{III}$ subsystem. Within the framework of the developed approach, the key mechanisms governing the two relevant phenomena (spin crossover and ferromagnetism) and their interplay will be revealed. In particular, the influence of the CH_2Cl_2, CH_2Br_2, and $CHBr_3$ solvents will be discussed.

2. Theoretical Model. To explain the long-range ordering that takes place in the $[Mn^{II}Cr^{III}(ox)_3]$ subsystem and the spin crossover transition demonstrated by the interacting $[Fe(sal_2\text{-trien})]^+$ complexes, we write down the Hamiltonian of the system in the following form

$$H = V_{ee} + H_{CF} + H_{SO} + H_{st} + H_{ex} + H_{Ze} \quad (1)$$

where the first term represents the interelectronic repulsion inside each iron ion, the second term is the crystal field that splits the ls-$^2T_2$ (t_2^5) term and shifts the hs-$^6A_1$ ($t_2^3e^2$) term of the Fe^{III} ions. This low symmetry crystal field of intermediate strength is induced by the nearest surrounding of the Fe^{III} ion consisting of 4 nitrogen and 2 oxygen ions. The third term is the spin−orbit interaction operating within the ls-$^2T_2$ terms, and the fourth term is the interaction of the Fe^{III} ions with the spontaneous all-round full symmetric lattice strain.[23−26] The exchange interaction between the Cr^{III} and Mn^{II} ions in the $[MnCr(ox)_3]^-$ subsystem is described by the fifth term. Finally, the last term of the Hamiltonian is the Zeeman interaction of the magnetic Fe^{III}, Cr^{III} and Mn^{II} ions. Because the ferromagnetic ordering in the Mn−Cr subsystem and the spin crossover in the Fe^{III} species take place in different temperature ranges, namely, at several K and 100−200 K, respectively, the interaction between these two subsystems is not included into consideration.

The energy gap between the hs-$^6A_1$ and ls-$^2T_2$ states in an isolated Fe^{III} is determined by the intraion Coulomb interaction and the crystal field that splits the ls-$^2T_2$ term. For the proper determination of this gap one needs first to take into account the Coulomb interaction mixing the ten $^2T_2$ terms arising from different $t_2^ne^{5-n}$ (n = 1−5) electronic configurations,[36] as it was done for the spin crossover $Mn^{III}(d^4)$ ion in.[27] In general, this mixing should affect the energy of the lowest $^2T_2$ term arising from the t_2^5 configuration. However, the calculations of the crystal field splittings discussed below apparently show that the effect of mixing of the lowest $^2T_2$ (t_2^5) term with nine excited $^2T_2$ states by Coulomb interaction is relatively small and can be neglected. In this case the energy difference between the $^2T_2$ (t_2^5) and $^6A_1$ ($t_2^3e^2$) terms of a single Fe^{III} ion provided by the interelectronic repulsion inside each iron ion can be written as[36]

$$\Delta E = 15B + 10C \quad (2)$$

where for the free Fe^{III} ion the values of the Racah parameters are B = 1015 cm^{-1} and C = 4800 cm^{-1}. Because the Racah parameters in a crystal are reduced as compared to those for free ions because of the covalency of the metal−ligand bonds (the so-called nephelauxetic effect),[37] further in the calculations we take for the parameters B and C values that make up 60% of the free ion values.

The crystal field potential acting on the electronic shell of the Fe^{III} ion looks as

$$H_{CF} = \sum_{i,l,m} B_l^m C_l^m(\vartheta_i, \varphi_i) \quad (3)$$

where $C_l^m(\vartheta,\varphi) = [4\pi/(2l + 1)]^{1/2}Y_{l,m}(\vartheta,\varphi)$ with $Y_{l,m}(\vartheta,\varphi)$ being normalized spherical harmonics B_l^m being the parameters that depend on the geometry of the ligand surrounding. For calculation of these parameters, we employ the exchange charge model of the crystal field suggested in,[38−40] which has been applied to different systems in.[41−47] In this model, two contributions to the energy of the 3d electrons in the crystal field are taken into account, namely, the contribution arising from the interaction of the 3d electrons with the point charges (pc) of the surrounding ligands and the contribution coming from the overlap of the 3d and ligand orbitals. The latter is referred to as the contribution of the exchange charges (ec). In the accepted crystal field model the parameters B_l^m look as follows

$$B_l^m = B_l^{m(pc)} + B_l^{m(ec)} \quad (4)$$

with

dx.doi.org/10.1021/ic401997w | Inorg. Chem. 2013, 52, 13536−13545

$$B_l^{m(\mathrm{pc})} = \sum_p \frac{Z_p e^2 \langle r^l \rangle}{(R_p)^{l+1}} C_l^{m*}(\vartheta_p, \varphi_p) \quad (5)$$

and

$$B_l^{m(\mathrm{ec})} = \frac{2e^2(2l+1)}{5} \sum_p \frac{S_l(R_p)}{R_p} C_l^{m*}(\vartheta_p, \varphi_p) \quad (6)$$

In eqs 5 and 6, the summation runs over all nearest ligands, $Z_p e$ is the effective charge of the pth ligand, which is approximately identified with the oxidation state of the ligand in the subsequent calculations. Finally, $S_l(R_p)$ are the overlap integrals. We employ the simplest version of the exchange charge model with the only phenomenological parameter G[39,40] in which the parameters $S_l(R_p)$ are written as

$$S_l(R_p) = G[S_s^2(R_p) + S_\sigma^2(R_p) + \gamma_l S_\pi^2(R_p)],\ \gamma_2 = 1,\ \gamma_4 = -4/3 \quad (7)$$

and $S_s(R_p) = \langle 3\mathrm{d},\ m = 0 | 2\mathrm{s} \rangle$, $S_\sigma(R_p) = \langle 3\mathrm{d},\ m = 0 | 2\mathrm{p},\ m = 0 \rangle$ $S_\pi(R_p) = \langle 3\mathrm{d},\ m = \pm 1 | 2\mathrm{p},\ m = \pm 1 \rangle$ are the overlap integrals of the 3d wave functions of Fe^{III} and 2s, 2p functions of nitrogen and oxygen ligands. The combinations $S_l(R)$ of the overlap integrals have been computed using the radial atomic "double-ζ" 3d wave functions of iron and 2s, 2p functions of nitrogen and oxygen given in ref 48. For the radial integrals, the values $\langle r^2 \rangle = 1.15 a_0^2$ and $\langle r^4 \rangle = 2.789 a_0^4$ (a_0 is the Bohr radius) have been used.[49] The parameter G will be determined further on from the optimal coincidence of the experimental and calculated data on the magnetic susceptibility.

The spin−orbit interaction for the ls-Fe^{III} ion is written as

$$H_{\mathrm{SO}} = \kappa\zeta \sum_i l_i s_i \quad (8)$$

where $\zeta = 486\ \mathrm{cm}^{-1}$ is the one-electron spin−orbit coupling constant[49] and κ is the orbital reduction factor. To reduce the number of free parameters, in the subsequent consideration we used the usually accepted value of $\kappa = 0.8$.

The combined action of the low-symmetry crystal field and the spin−orbital interaction leads to the splitting of the ls-$^2T_2$ state of the Fe^{III} ion into three Kramers doublets with the ground doublet separated from the two excited ones by the energy gaps exceeding significantly the thermal energy $k_B T$ (see section 3). Therefore, further on, we suppose that in the spin conversion two levels of a single Fe^{III} ion participate, namely, the hs-$^6A_1$ term and the low-lying Kramers doublet arising from the ls-$^2T_2$ term. Following refs 23−26, we assume that the mechanism responsible for the ls-hs transition is the interaction of the Fe^{III} ions with the spontaneous totally symmetric lattice strain (electron−deformational interaction). In the basis of the indicated two states, the Hamiltonian of electron−deformational interaction can be written as (for details, see refs 23−26) follows

$$H_{\mathrm{st}} = -b \sum_k \tau_k - \frac{J}{2N} \sum_{k,k'} \tau_k \tau_{k'} \quad (9)$$

with $b = A\upsilon_1\upsilon_2$, $J = A\upsilon_1^2$ and

$$A = \frac{c_2}{c_1[c_2\Omega_0 + c_1(\Omega - \Omega_0)]} \quad (10)$$

here, Ω_0 is the volume which falls per one Fe^{III} ion and its nearest environment and Ω is the unit-cell volume, N is the number of unit cells in the crystal, c_1 and c_2 are the elastic bulk moduli corresponding to the internal molecular (FeN_4O_2) and external (intermolecular volume) strains, $\upsilon_1 = (\upsilon_{\mathrm{hs}} - \upsilon_{\mathrm{ls}})/2$, $\upsilon_2 = (\upsilon_{\mathrm{hs}} + \upsilon_{\mathrm{ls}})/2$, υ_{hs} and υ_{ls} are the constants of interaction with the full symmetric strain of the hs-$^6A_1$ state and the lowest in energy Kramers doublet arising from the ls-$^2T_2$ state, τ_k is a diagonal matrix of the dimension 8 × 8 with the matrix elements 1 and −1 corresponding to the hs-state $^6A_1$ and the mentioned ls Kramers doublet, respectively. The coupling to the strain gives rise to an infinite range interaction between all molecules in the crystal. This intermolecular interaction corresponds to the exchange via the field of long-wave acoustic phonons.[50] Further on, we also include in the Hamiltonian H_{st} the term

$$\frac{\Delta}{2} \sum_k \tau_k \quad (11)$$

where Δ is the energy gap between the two hs- and ls-states involved in consideration. The parameters b and Δ will be calculated further on within the exchange charge model and expressed in terms of its phenomenological parameter G (see section 3).

The exchange interaction between the Cr^{III} and Mn^{II} ions in the $[MnCr(ox)_3]^-$ subsystem is written as

$$H_{\mathrm{ex}} = -2 \sum_{i,j} J_{ij}^{\mathrm{ex}} \mathbf{S}_{\mathrm{Mn}}^i \mathbf{S}_{\mathrm{Cr}}^j \quad (12)$$

where the summation over i and j includes all ions between which the exchange interaction takes place.

Then the molecular field approximation is applied for the electron-deformational long-range and exchange interactions, and the quantities $\tau_k\tau_{k'}$ and $\mathbf{S}_{\mathrm{Mn}}^i \mathbf{S}_{\mathrm{Cr}}^j$ in eqs 9 and 12, respectively, are replaced by

$$\tau_k\tau_{k'} = \langle\tau\rangle\tau_k + \langle\tau\rangle\tau_{k'} - \langle\tau\rangle^2$$

$$S_{\mathrm{Mn}}^{i\alpha} S_{Cr}^{j\alpha} = \langle S_{\mathrm{Mn}}^\alpha \rangle S_{\mathrm{Cr}}^{j\alpha} + S_{\mathrm{Mn}}^{i\alpha} \langle S_{\mathrm{Cr}}^\alpha \rangle - \langle S_{\mathrm{Mn}}^\alpha \rangle \langle S_{\mathrm{Cr}}^\alpha \rangle,\ (\alpha = x, y, z) \quad (13)$$

$$\langle\tau\rangle \equiv \bar{\tau} = \mathrm{Tr}(\exp(-\tilde{H}/k_B T)\tau_k)/\mathrm{Tr}(\exp(-\tilde{H}/k_B T))$$

$$\langle S_{\mathrm{Mn}}^\alpha \rangle \equiv \bar{S}_{\mathrm{Mn}}^\alpha = \mathrm{Tr}(\exp(-\tilde{H}/k_B T) S_{\mathrm{Mn}}^{i\alpha})/\mathrm{Tr}(\exp(-\tilde{H}/k_B T))$$

$$\langle S_{\mathrm{Cr}}^\alpha \rangle \equiv \bar{S}_{\mathrm{Cr}}^\alpha = \mathrm{Tr}(\exp(-\tilde{H}/k_B T) S_{\mathrm{Cr}}^{j\alpha})/\mathrm{Tr}(\exp(-\tilde{H}/k_B T)) \quad (14)$$

where k_B is the Boltzmann constant and $\tilde{H}$ is the total Hamiltonian of the system in the molecular field approximation that represents Hamiltonian, eq 1, in which the interactions H_{st} and H_{ex} have been substituted by

$$\tilde{H}_{\mathrm{st}} = -\left(J\bar{\tau} + b - \frac{\Delta}{2}\right) \sum_k \tau_k,\ H_{\mathrm{ex}} = -2J_{ex} \sum_{j,\alpha} \bar{S}_{\mathrm{Mn}}^\alpha S_{\mathrm{Cr}}^{j\alpha} - 2J_{\mathrm{ex}} \sum_{i,\alpha} \bar{S}_{\mathrm{Cr}}^\alpha S_{\mathrm{Mn}}^{i\alpha} \quad (15)$$

where $J_{\mathrm{ex}} = \sum_j J_{ij}$. In the mean field approximation for temperatures higher than the phase transition temperature T_C the magnetic susceptibility χ of the $[MnCr(ox)_3]$ network per a Mn−Cr pair is described by the expression

dx.doi.org/10.1021/ic401997w | Inorg. Chem. 2013, 52, 13536−13545

Table 1. Spherical Coordinates of the Ligand Surrounding of the Fe^{III} Ion in the Compounds $1{\cdot}CH_2Cl_2$ $1{\cdot}CH_2Br_2$, and $1{\cdot}CHBr_3$

		ligands					
compd	spherical coordinates of the ligands	O1	O2	N1	N2	N3	N4
$1{\cdot}CH_2Cl_2$	R (Å)	1.86	1.87	1.95	2.02	2.03	1.95
	θ (deg)	93	87	0	84	98	179
	φ (deg)	96	0	0	270	186	354
$1{\cdot}CH_2Br_2$	R (Å)	1.87	1.85	1.94	2.03	2.02	1.94
	θ (deg)	92	87	0	84	96	179
	φ (deg)	96	0	0	270	186	117
$1{\cdot}CHBr_3$	R (Å)	1.88	1.87	1.98	2.06	2.05	1.98
	θ (deg)	91	88	0	82	99	178
	φ (deg)	103	0	0	272	191	80

Table 2. Overlap Integrals $S_l(R_i)$ and Their Derivatives $S'_l(R_i) = dS_l(R_i)/dR_i$ (in a_0^{-1})* for $1{\cdot}CH_2Cl_2$, $1{\cdot}CH_2Br_2$, and $1{\cdot}CHBr_3$

		ligands					
compd	overlap integrals and their derivatives	O1	O2	N1	N2	N3	N4
$1{\cdot}CH_2Cl_2$	$S_2(R)$	0.01722	0.01648	0.01533	0.01214	0.01202	0.01533
	$S_4(R)$	0.01123	0.01084	0.00977	0.00811	0.00804	0.00977
	$S'_2(R)$	−0.03074	−0.02960	−0.02528	−0.02072	−0.02055	−0.02528
	$S'_4(R)$	−0.01611	−0.01579	−0.01255	−0.01135	−0.01129	−0.01255
$1{\cdot}CH_2Br_2$	$S_2(R)$	0.01651	0.01792	0.01580	0.01202	0.01214	0.01580
	$S_4(R)$	0.01085	0.01159	0.01000	0.00804	0.00811	0.01000
	$S'_2(R)$	−0.02965	−0.03181	−0.02593	−0.02055	−0.02072	−0.02593
	$S'_4(R)$	−0.01580	−0.01640	−0.01268	−0.01129	−0.01135	−0.01268
$1{\cdot}CHBr_3$	$S_2(R)$	0.01614	0.01639	0.01402	0.01083	0.01124	0.01402
	$S_4(R)$	0.01065	0.01079	0.00911	0.00738	0.00760	0.00911
	$S'_2(R)$	−0.02908	−0.02947	−0.02344	−0.01877	−0.01938	−0.02344
	$S'_4(R)$	−0.01563	−0.01575	−0.01212	−0.01067	−0.01090	−0.01212

*a_0 is the Bohr radius

$$\chi_{Cr-Mn} = \frac{T(C_1 + C_2) + 2C_1C_2\gamma}{T^2 - T_C^2} \quad (16)$$

where

$$C_i = \frac{Ng^2\mu_B^2 S_i(S_i + 1)}{2k_B} \quad (17)$$

with $S_1 = 3/2$ and $S_2 = 5/2$ being the spins of Cr^{III} and Mn^{II} ions, respectively, and

$$\gamma = \frac{16}{3k_B}\frac{J_{ex}}{g^2},\ T_C = \gamma\sqrt{C_1C_2}. \quad (18)$$

N, μ_B are the Avogadro number and Bohr magneton, respectively.

As it was mentioned above the $Mn^{II}-Cr^{III}$ and Fe^{III} subsystems do not interact, and therefore, the magnetic susceptibility of the crystal can be calculated as a sum of the susceptibilities of each subsystem

$$\chi = \chi_{Cr-Mn} + \chi_{Fe} \quad (19)$$

Further on, the magnetic susceptibility of the $[MnCr(ox)_3]$ network is calculated with the aid of eq 16. The magnetic susceptibility of a $[Fe(sal_2\text{-trien})]^+$ complex in the molecular field approximation can be represented as

$$\chi_{Fe} = n(Fe^{III}_{hs})\chi(Fe^{III}_{hs}) + n(Fe^{III}_{ls})\chi(Fe^{III}_{ls}) \quad (20)$$

where the temperature dependences of the $n(Fe^{III}_{hs})$ and $n(Fe^{III}_{ls})$ fractions are calculated within the framework of the developed model. For the hs-$^6A_1$ term of the Fe^{III} ion the orbital angular momentum is completely quenched and the Fe^{III} ion in this state can be regarded as a pure spin $S = 5/2$ ion. The magnetic susceptibility in this case is calculated as

$$\chi(Fe^{III}_{hs}) = \frac{Ng^2\mu_B^2}{3k_BT}S(S + 1)\cdot \quad (21)$$

Owing to the peculiarities of the energy spectrum of the *ls*- Fe^{III} ion the susceptibility $\chi(Fe^{III}_{ls})$ is calculated taking into account the lowest Kramers doublet of this ion (see Section 3) generated by the crystal field and spin−orbital interaction.

3. DISCUSSION

We start with the discussion of the energy level diagrams for the Fe^{III} ion in the series $1{\cdot}CH_2Cl_2$, $1{\cdot}CH_2Br_2$ and $1{\cdot}CHBr_3$. With this aim we calculate the energies of three Kramers doublets arising from the splitting of the ls-$^2T_2$ term by the crystal field and spin−orbit interaction. As was mentioned above, the local neighborhood of the Fe^{III} ion in the compounds under examination consists of 4 nitrogen and 2 oxygen atoms. The spherical coordinates of these atoms with respect to the central Fe^{III} ion placed at the origin of the coordinate system are given in Table 1. From Table 1, it is seen that the radia and the angles θ and φ determining the position of the ligands of the Fe^{III} ion slightly differ for the $1{\cdot}CH_2Cl_2$, $1{\cdot}CH_2Br_2$, and $1{\cdot}CHBr_3$ compounds. The small difference is most probably caused by the solvents. At the same time, it is worth noting that the solvent affects insignificantly the structure of the first coordination sphere of the spin crossover ions.

With the aid of the formulas 3−7, the crystal field Hamiltonian acting within the space of the 3d orbitals of the

dx.doi.org/10.1021/ic401997w | Inorg. Chem. 2013, 52, 13536−13545

Fe^{III} ion in the mentioned compounds can be written in the following form

$$H_{CF} = \sum_{l=2,4,6} a_l^0 Y_{l,0}(\theta, \varphi) + \sum_{l=2,4,6} \sum_{m=1}^{l} \{a_l^m [Y_{l,-m}(\theta, \varphi) + (-1)^m Y_{l,m}(\theta, \varphi)] + ib_l^m [Y_{l,-m}(\theta, \varphi) + (-1)^{m+1} Y_{l,m}(\theta, \varphi)]\} \quad (22)$$

The combinations of the overlap integrals $S_2(R_p)$,$S_4(R_p)$ necessary for the calculation of the crystal field parameters a_l^m and b_l^m are listed in Table 2. In calculations of the crystal field parameters for oxygen and nitrogen ligands, the formal charges −1 and 0 were taken, respectively.

The contributions to the crystal field parameters a_l^m and b_l^m that come from the point and exchange charges were calculated with the aid of expressions 3−7 and are given in Table 3. The

Table 3. Crystal Field Parameters (in cm^{-1}) for 1·CH_2Cl_2, 1·CH_2Br_2, and 1·$CHBr_3$

	compd					
	1		2		3	
crystal field params	point	exchange	point	exchange	point	exchange
a_2^0	−9033	391 G	−9155	476 G	−8947	176 G
a_2^1	678	533 G	676	567 G	444	518 G
b_2^1	−655	−497 G	−442	−472 G	−147	−439 G
a_2^2	19	−103 G	333	273 G	547	173 G
b_2^2	−1216	−153 G	−1159	−129 G	−2325	−453 G
a_4^0	963	8314 G	990	8568 G	960	7677 G
a_4^1	−133	−785 G	−136	−606 G	−87	−675 G
b_4^1	130	608 G	87	432 G	29	173 G
a_4^2	4	70 G	−39	−126 G	−48	−78 G
b_4^2	112	96 G	107	80 G	215	294 G
a_4^3	68	510 G	88	487 G	55	420 G
b_4^3	110	676 G	74	575 G	21	623 G
a_4^4	1313	4796 G	1346	4892 G	1105	3948 G
b_4^4	296	1021 G	279	1045 G	516	1889 G

diagonalization of Hamiltonian, eq 22, along with the spin−orbit interaction, eq 8, in the basis of the ls-$^2T_2$ state leads to three Kramers doublets. For all three compounds the energies of these Kramers doublets as functions of the parameter G are shown in Figure 1. In the same figure the position of the hs-$^6A_1$ state is depicted. One can see that in the group of levels 1−3 originating from the ls-$^2T_2$ state, level 3 is the lowest one. The energy gaps between levels 2 and 3 are approximately equal to 1880, 1770, and 2770 cm^{-1} for 1·CH_2Cl_2, 1·CH_2Br_2, and 1·$CHBr_3$, respectively, and exceed significantly the thermal energy k_BT. At the same time for levels 1−3 the J-parameters for the electron-deformational interaction with the full symmetric strain, eq 9, are approximately proportional to $(\langle i|H_{cr}|i\rangle - \langle {}^6A_1|H_{cr}|{}^6A_1\rangle)^2/R^2$ [23,28] (where i = 1−3 and R is the mean distance between the Fe^{III} ion and the ligands), and they are expected to be very small as compared with the calculated energy gaps between these levels.[23,28] Thus, for a fixed energy level scheme (given G value) the electron-deformational interaction will not lead to any change in the order of levels 1−3 so as in the three examined systems only levels 3 and 4 will participate in the observed spin conversion. The influence of this interaction will be to modify the hs-ls gap Δ, eq 11, through the parameter b. These considerations based on the performed calculations (Figures 1−3) justify the accepted form of the operator of electron-deformational interaction, eq 9. Then, for the three compounds we calculate the G-dependence of the parameter $-2b$ (eq 9 and Figure 2) that allows us to redetermine the hs−ls gap Δ at the expense of electron−deformational interaction. The matrix elements υ_{hs} and υ_{ls} that contribute to $\upsilon_1$and υ_2 can be written in the form

$$\upsilon_{ls} = \langle 3| \left(\sum_i \frac{\partial W}{\partial R_i} R_i \right)_{R_i = R_i^{ls}} |3\rangle \frac{1}{\sqrt{3}}, \quad \upsilon_{hs} = \langle \text{hs-}{}^6A_1| \left(\sum_i \frac{\partial W}{\partial R_i} R_i \right)_{R_i = R_i^{hs}} |\text{hs-}{}^6A_1\rangle \frac{1}{\sqrt{3}} \quad (23)$$

where W is the electron−nuclear potential energy and i runs over all six ligands of the Fe^{III} ion. After substitution of the numerical values of the radii, overlap integrals and their derivatives (Table 3) into eq 23 we obtain that the matrix element υ_{ls} can be expressed in terms of the phenomenological parameter G of the exchange charge model, while the matrix element υ_{hs} is vanishing. The results presented in Figures 1 and 2 give the possibility to calculate the effective energy gap $\Delta - 2b$, eq 15, as a function of G. Figure 3 illustrates the energies of the low-lying levels renormalized by electron−deformational interaction as a function of G for 1·CH_2Cl_2 . It is seen that for G values at which the energy of the level 4 exceeds that of level 3 (spin crossover range), the gap Δ between these levels increases at the expense of cooperative interaction.

Further on, we calculate the magnetic susceptibility of a crystal consisting of the Fe^{III} and Mn−Cr subsystems. The magnetic susceptibility of the latter dominates the total susceptibility of the crystal at low temperatures and it is quite well described by expression 16 using the J_{ex} values given in Table 4. At intermediate and high temperatures the χT contribution of the Mn−Cr subsystem stays almost constant, while in this range the χT contribution of the Fe^{III} subsystem changes as a consequence of the spin crossover. Thus, in this range the fitting procedure concerns the Fe^{III} subsystem and contains the following steps: First, for an initial value of the parameter G, the splitting of the ls-$^2T_2$ term of a single Fe^{III} ion produced by the common action of the crystal field and spin−orbital interaction is calculated, and the wave function and energy of the lowest Kramers doublet is determined. Then, because of the large energy gaps between the lowest in energy Kramers doublet and the excited ones (see Figure 1), we consider a two-level scheme containing this doublet and the hs-$^6A_1$ state and calculate the effective gap $\Delta - 2b$ between them for the mentioned G value and a definite value of J. The next step is the self-consistent procedure for evaluation of the temperature dependence of $\bar{\tau}$ (see eq 14). At the second stage the product $\chi_{Fe}T$ is calculated with the aid of eq 20, and the χT values, eq 19, are compared with the experimental ones. The procedure of calculation of $\bar{\tau}$ and χT is repeated until for certain values of parameters G and J the optimal coincidence between the calculated and experimental χT curves is obtained.

The temperature dependence of the magnetic susceptibility for the three compounds under examination is presented in Figure 4. The calculated curves are in excellent agreement with the observed ones as confirmed by the agreement criterion defined as $(\sum((\chi T_{theor})_i/(\chi T_{exp})_i - 1)^2/N)^{1/2}$, which is equal to 3.8, 5.2, and 4.7% for 1·CH_2Cl_2, 1·CH_2Br_2, and 1·$CHBr_3$,

dx.doi.org/10.1021/ic401997w | Inorg. Chem. 2013, 52, 13536−13545

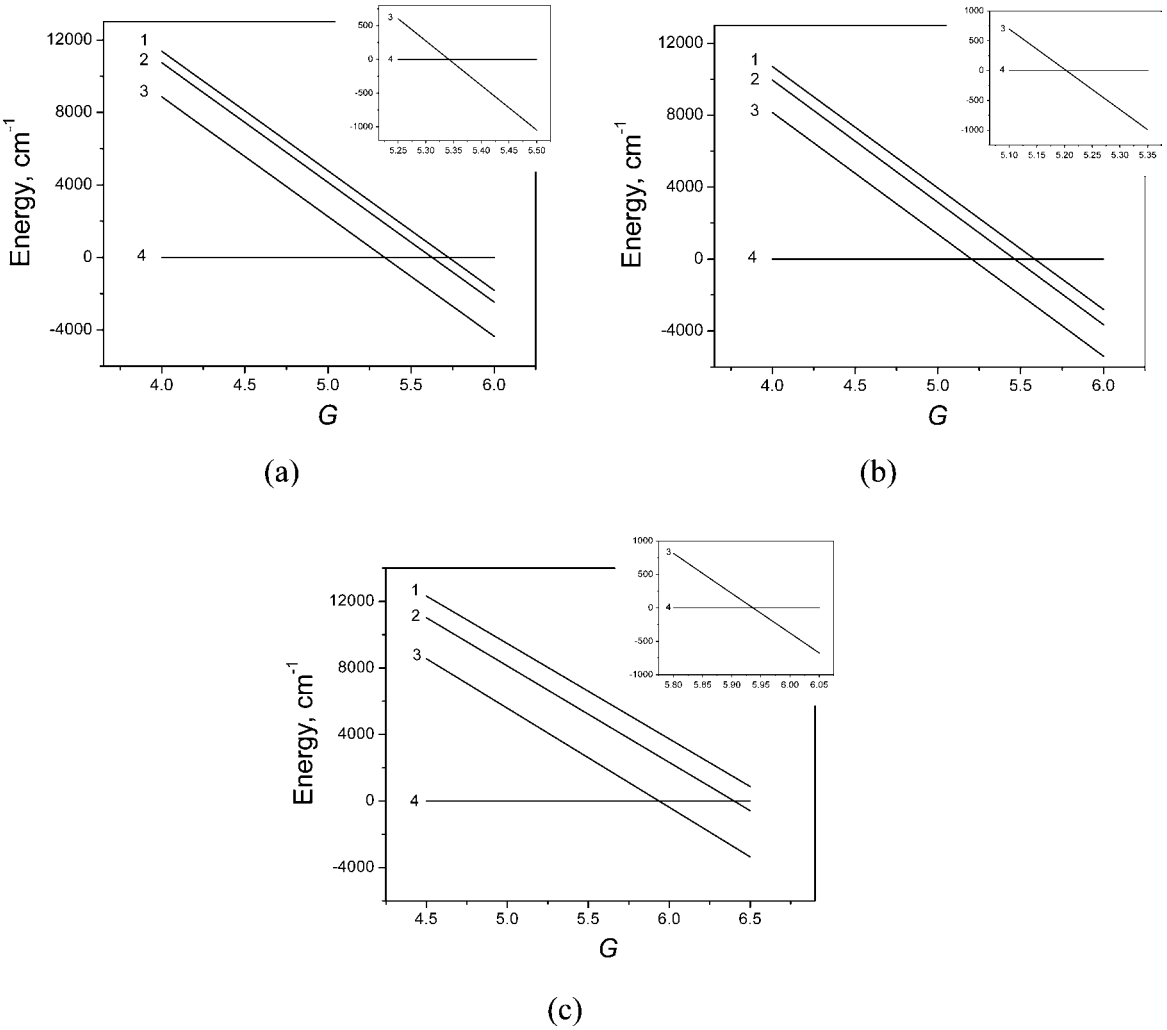

Figure 1. Energy levels of a single Fe^{III} ion calculated as functions of the parameter G of the exchange charge model for (a) **1**·CH_2Cl_2, (b) **1**·CH_2Br_2, and (c) **1**·$CHBr_3$. Curves 1−3 describe the energies of the Kramers doublets arising from the ls-$^2T_2$ state and counted off from the energy of the hs-$^6A_1$ state (curve 4). The ranges of parameters G wherein the spin crossover takes place are shown in the insets.

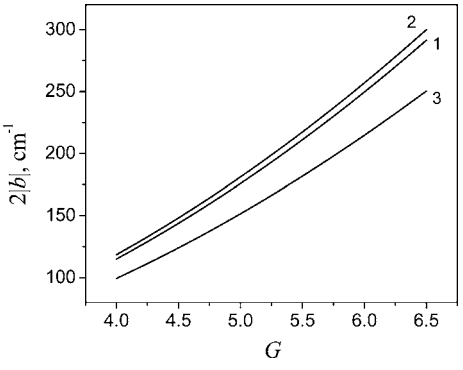

Figure 2. Values 2|b| as functions of the G parameter calculated for **1**·CH_2Cl_2 (curve 1), **1**·CH_2Br_2 (curve 2), and **1**·$CHBr_3$ (curve 3).

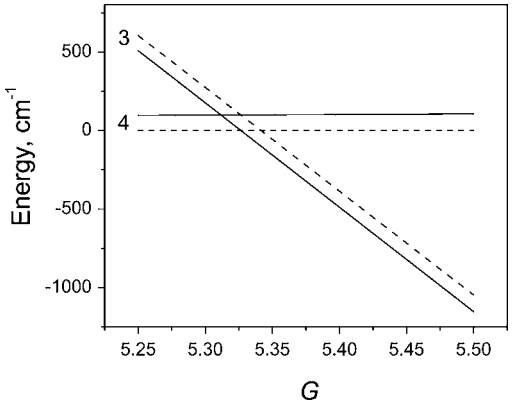

Figure 3. Change in the energy gap between levels 3 and 4 at the expense of cooperative interaction in **1**·CH_2Cl_2; solid lines are the energy levels redetermined by taking into account the electron−deformational interaction; dashed lines are the crystal field levels.

respectively. To understand with utmost clarity the magnetic behavior of the systems under examination in Figure 5, we present the ratio n_{hs}/n_{ls} as a function of temperature. It is seen that for **1**·$CHBr_3$ the hs fraction starts increasing at considerably lower temperature than for **1**·CH_2Cl_2 and **1**·CH_2Br_2. However, for all compounds the increase of the hs fraction is gradual and in fact the temperature dependence of this fraction resembles that of the magnetic susceptibility. It is also seen that for compounds **1**·CH_2Cl_2 and **1**·CH_2Br_2 the increase of the hs fraction occurs at much higher temperatures.

The parameters obtained in fitting of the magnetic properties are given in Table 4. It is seen that for all three compounds the

dx.doi.org/10.1021/ic401997w | Inorg. Chem. 2013, 52, 13536−13545

Table 4. Best Fit Parameters for 1·CH_2Cl_2, 1·CH_2Br_2, and 1·$CHBr_3$

compd	G	J (cm^{-1})	J_{ex} (cm^{-1})
1·CH_2Cl_2	5.34	152.8	1.45
1·CH_2Br_2	5.2	128.7	1.42
1·$CHBr_3$	5.92	34.0	1.42

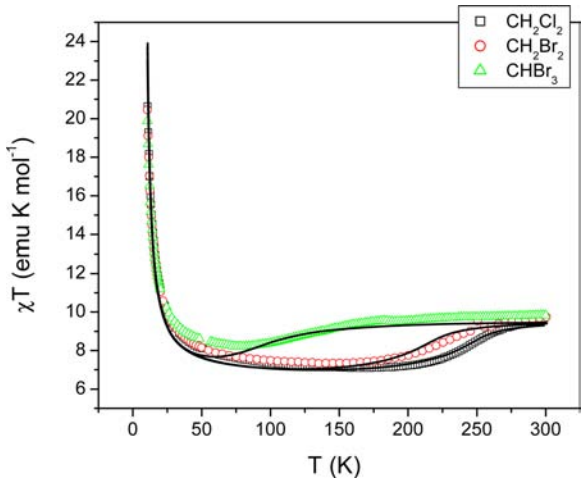

Figure 4. Temperature dependence of the magnetic susceptibility for 1·CH_2Cl_2, 1·CH_2Br_2, and 1·$CHBr_3$: symbols, experiment; solid lines, theoretical curves calculated with the parameters given in Table 4.

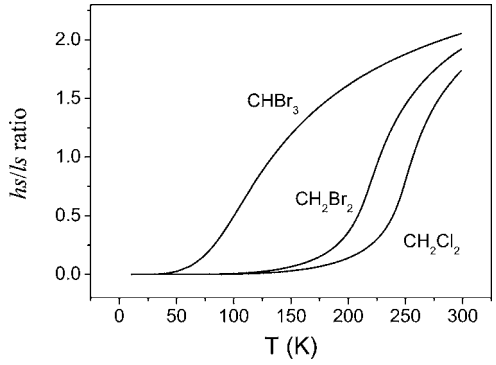

Figure 5. Ratio n_{hs}/n_{ls} as a function of temperature for 1·CH_2Cl_2, 1·CH_2Br_2, and 1·$CHBr_3$ calculated with the parameters given in Table 4.

obtained G values are slightly larger than those for which the intersection of the hs-$^6A_1$ state and the lowest in energy Kramers doublet occurs. For these G values the ls state is lower in energy than the hs one in all compounds. At the same time the negative b values lead to an increase in the effective ls−hs gap $\Delta - 2b$. Upon heating, the cooperative interaction via the field of long-wave acoustic phonons brings together the hs and ls levels, and the gradual spin crossover takes place. The parameter of electron-deformational interaction J decreases in the order 1·CH_2Cl_2 > 1·CH_2Br_2 > 1·$CHBr_3$. This decrease in J is most probably facilitated by the increase in the elasticity of the space between the iron ions in the examined series of compounds and it may be connected with the larger ionic radius of bromine. The exchange interaction within $[MnCr(ox)_3]^-$ subsystem was found to be ferromagnetic with similar exchange parameters for all compounds under study that reflects the fact that this subsystem is the same in all crystals.

The obtained results also give the possibility to explain qualitatively the change in the so-called temperature T_{LIESST}[35b] of the LIESST effect[51] in the examined Fe^{III} compounds. The single coordinate configuration model presents the energy spectrum of an isolated Fe^{III} ion by two parabolic adiabatic potential sheets, corresponding to the lowest in energy Kramers doublet (ls-state) and the hs $^6A_1$ state. Within this model the barrier height (activation energy E_A) between these states is given by the expression

$$E_A = \frac{\omega\Delta^2}{2V_{ls}^2} \tag{24}$$

where Δ has the same sense as in eq 11, $V_{ls} = \frac{\upsilon_{ls}}{R}\frac{\sqrt{\hbar\omega}}{2f}$ is the constant of interaction of the ls state with the breathing mode of the nearest environment of the Fe^{III} ion in the ls state, f is the force constant of the breathing mode, and ω is its frequency. Since the parameter of electron- deformational interaction $J = A\upsilon_{ls}^2$ decreases in the series of compounds 1·CH_2Cl_2, 1·CH_2Br_2, and 1·$CHBr_3$ (Table 4) one immediately obtains that the activation energy E_A and, hence, T_{LIESST} follows the opposite trend and thus increases in the order 1·CH_2Cl_2 < 1·CH_2Br_2 < 1·$CHBr_3$. This result is in line with the experimental data obtained in.[35b] Thus, the presented model describes correctly not only the thermal spin crossover but also the tendency in the change of the temperature T_{LIESST} in the mentioned compounds.

Recently, an assumption has been expressed that along with the contribution of the breathing mode to the activation energy E_A the coupling with the bending vibrations is also relevant for the LIESST effect in Fe^{III} compounds.[52] On the basis of this assumption in paper,[35b] it was concluded that the $[Fe^{III}(sal_2\text{-}trien)]^+$ compounds exhibiting a LIESST effect present a large distortion of the octahedral geometry in their hs state. However, the hs $^6A_1$ state can interact only with full symmetric vibrations in accordance with the group theoretical selection rules, and, hence, the low symmetry modes cannot lead to any additional shift of the minimum of the adiabatic potential. In contrast, the ls state of the Fe^{III} ion, $^2T_2$, can interact with vibrations other than the full symmetric one. Hence, one can expect that deviations from the cubic symmetry can lead to a shift of the minimum of the adiabatic potential for the ls state. Still, experimentally[35] the trigonal prismatic distortion in the ls state is much smaller than for the hs state. Thus, one can conclude that the inclusion of nonsymmetric modes in the model will not bring to noticeable increase in activation energy E_A. This probably explains the fact that some spin-crossover Fe^{III} compounds, such as the ClO_4^- derivative and the 3D $[Mn^{II}Cr^{III}(ox)_3]^-$ salt, do not present a LIESST effect[35] in spite of strong distortion of the octahedral geometry. In the three compounds presented in the present paper the LIEEST effect observed should be therefore attributed most probably to confinement of the Fe^{III} complexes in between the bimetallic layers and not to the strong distortion of the hs Fe^{III} state.

Mössbauer spectra provide a direct measurement of the population of the hs and ls states and serve as a reliable test for the theoretical background of the spin crossover phenomenon. We assume that each type of iron ion in the sample is represented in the Mössbauer spectrum by a quadrupole doublet, each doublet being the superposition of two Lorenz curves. The Mössbauer spectrum observed is obtained by summing up the spectra yielded by different electronic states in molecular field, taking into account their equilibrium populations for a given value of the molecular field at a certain

dx.doi.org/10.1021/ic401997w | Inorg. Chem. 2013, 52, 13536−13545

temperature. The shape function of the Mössbauer spectra produced by Fe^{III} ions in the ls and hs states is determined by superposition of the Lorenz curves

$$F_C(\Omega) = n(Fe^{III}_{hs}) \sum_{\pm} \frac{\Gamma_{Fe^{III}_{hs}}}{(\Gamma_{Fe^{III}_{hs}})^2 + (\Omega - \delta_{Fe^{III}_{hs}} \pm \Delta E_{Fe^{III}_{hs}}/2)^2} + n(Fe^{III}_{ls}) \sum_{\pm} \frac{\Gamma_{Fe^{III}_{ls}}}{(\Gamma_{Fe^{III}_{ls}})^2 + (\Omega - \delta_{Fe^{III}_{ls}} \pm \Delta E_{Fe^{III}_{ls}}/2)^2} \quad (25)$$

In eq 25, the temperature dependence of the $n(Fe^{III}_{hs})$ and $n(Fe^{III}_{ls})$ fractions are calculated within the framework of the developed model, $\Delta E_{Fe^{III}_{hs}}$, $\Delta E_{Fe^{III}_{ls}}$ and $\delta_{Fe^{III}_{hs}}$, $\delta_{Fe^{III}_{ls}}$ are the quadrupole splittings and isomer shifts in the hs and ls states, respectively.

The simulated Mössbauer spectra for $\mathbf{1}\cdot CH_2Cl_2$ in a wide temperature range are shown in Figure 6 together with the

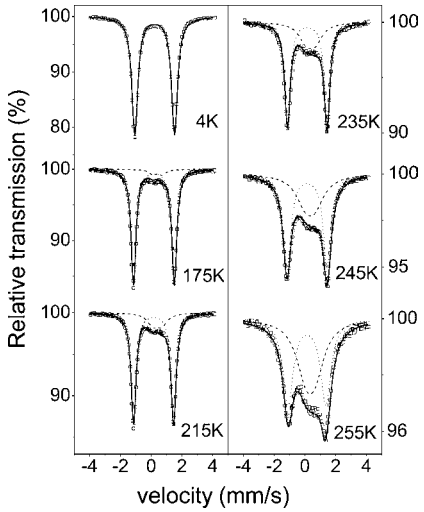

Figure 6. Mössbauer spectra of $\mathbf{1}\cdot CH_2Cl_2$. Points, experimental data; thick solid lines, theoretical calculations. Contributions from hs and ls Fe^{III} ions are shown with dashed and dotted lines, respectively.

experimental ones. Quite good agreement is obtained between the observed and calculated spectra at all temperatures. Values of the quadrupole splittings, isomer shifts and line widths used in this simulation are given in Table 5. At low temperature, the spectrum contains a doublet characteristic of the ls-Fe^{III} ions.

Table 5. Mössbauer Parameters for the Fe^{III} Ions in $\mathbf{1}\cdot CH_2Cl_2$

T (K)		IS (mm/s)	QS (mm/s)	Γ (mm/s)
4	hs			
	ls	0.23	2.58	0.48
175	hs	0.42	0.6	0.6
	ls	0.18	2.65	0.39
215	hs	0.40	0.6	0.86
	ls	0.16	2.6	0.4
235	hs	0.38	0.62	1.1
	ls	0.15	2.57	0.44
245	hs	0.35	0.62	1.51
	ls	0.14	2.61	0.62
255	hs	0.34	0.61	1.5
	ls	0.13	2.45	0.81

With the temperature increase, the amount of hs Fe^{III} ions increases. This leads to noticeable changes in the Mössbauer spectra, and at room temperature the doublet corresponding to the hs Fe^{III} ions makes up a significant part of the total spectra intensity. The percentages of hs and ls Fe^{III} ions determined from the calculated and observed Mössbauer spectra are listed in Table 6. From Figure 6 and Table 6, it follows that the

Table 6. Fraction of hs-Fe^{III} Ions Calculated Theoretically and Determined from the Experimental Mössbauer Spectra of $\mathbf{1}\cdot CH_2Cl_2$

	T (K)							
	4	165	175	195	215	235	245	255
expt (%)	0	6	8	11	16	24	42	50
theory (%)	0	4.6	6.2	10.8	17.8	29.9	39.2	48.9

developed theoretical model gives a reasonable estimation of the partial contributions of ls and hs Fe^{III} ions to the Mössbauer spectra. The developed model also provides satisfactory explanation of the Mössbauer spectra of $\mathbf{1}\cdot CH_2Br_2$ and $\mathbf{1}\cdot CHBr_3$. For these crystals in Tables 7 and 8, the calculated

Table 7. Fraction of *hs*-Fe^{III} ions calculated theoretically and determined from the experimental Mössbauer spectra of $\mathbf{1}\cdot CH_2Br_2$

	T (K)				
	77	160	180	199	245
expt (%)	0	10	15	22	73
theory (%)	0	8.4	15.1	25.6	57.8

fractions of hs Fe^{III} ions and those determined from the experimental Mössbauer spectra are compared. A reasonable agreement between the experimental data and theoretical calculations is obtained using the same set of parameters we have used to explain the magnetic properties of the three compounds under study.

4. CONCLUDING REMARKS

In this article, we have presented a microscopic approach to describe the behavior of multifunctional hybrid materials which demonstrate spin crossover phenomenon and ferromagnetic ordering. The ls−hs transition was considered as a cooperative phenomenon that is driven by the interaction of electronic shells of Fe^{III} ions with the fully symmetric deformation of the local coordination environment that is extended over the crystal lattice via the acoustic phonon field. The ferromagnetic exchange interaction was shown to be responsible for the magnetic ordering in the Mn−Cr subsystem. The crystal field together with the spin−orbital interaction were demonstrated to form the energy spectrum of the ls-Fe^{III} ion. The energy levels of the isolated Fe^{III} ions were calculated in the framework of the exchange charge model of the crystal field for the real symmetry of the nearest ligand surrounding. The developed approach was applied to the analysis of the behavior of a series of three compounds, namely, $[Fe^{III}(sal_2\text{-trien})][Mn^{II}Cr^{III}(ox)_3]\cdot solv$, where solv = CH_2Cl_2, CH_2Br_2, and $CHBr_3$. The spin transitions were treated within the molecular field approximation. For all three complexes under study, we were able to interpret qualitatively and quantitatively a wide set of the experimental data on the temperature dependence of magnetic

dx.doi.org/10.1021/ic401997w | Inorg. Chem. 2013, 52, 13536−13545

Table 8. Fraction of hs-Fe^{III} Ions Calculated Theoretically and Determined from the Experimental Mössbauer Spectra of the 1·$CHBr_3$

	T (K)							
	77	100	130	170	190	210	230	250
expt (%)	18	28	43	66	72	73	78	85
theory (%)	15.7	33.2	48.7	58.1	60.7	62.6	64.1	65.3

susceptibility and Mössbauer spectra with a unified set of parameters. The performed calculations apparently show a recognizable trend in the magnetic and spectroscopic behaviors induced by different solvent molecules. The softer the intermolecular space the more pronounced is the change in the magnetic properties expressed in a faster increase of the magnetic susceptibility which starts at lower temperature. In the series of compounds 1·CH_2Cl_2, 1·CH_2Br_2, and 1·$CHBr_3$, these temperatures and the χT values in whole temperature range follow the trends T (1·$CHBr_3$) < T (1·CH_2Br_2) < T (1·CH_2Cl_2) and χT(1·$CHBr_3$) > χT(1·CH_2Br_2) > χT(1·CH_2Cl_2).

In the framework of the developed model, we also provided a qualitative discussion of the LIESST effect in this series. More detailed quantitative description of this phenomenon is under way.

AUTHOR INFORMATION

Corresponding Author

*E-mail: klokishner@yahoo.com.

Notes

The authors declare no competing financial interest.

ACKNOWLEDGMENTS

The financial support of EU (ERC Advanced Grant SPINMOL, COST Action POCHEMON), Spanish MINECO (Consolider Molecular Nanoscience, MAT2011-22785), Generalidad Valenciana (PROMETEO and ISIC-Nano Programs) is highly appreciated. A.V.P thanks the University of Valencia for a visiting research grant. S.M.O, O.S.R., A.V.P, and S.I.K. thank the Supreme Council for Science and Technological Development of the Republic of Moldova, project 11.817.05.03A, for support.

REFERENCES

(1) Cambi, L.; Szego, L. *Ber. Dtsch. Chem. Ges.* **1931**, *64*, 2591.
(2) Cambi, L.; Szego, L. *Ber. Dtsch. Chem. Ges.* **1933**, *66*, 656.
(3) Gütlich, P.; Garcia, Y.; Goodwin, H. A. *Chem. Soc. Rev.* **2000**, *29*, 419. Gütlich, P.; Ksenofontov, V.; Gaspar, A. B. *Coord. Chem. Rev.* **2005**, *249*, 1811. Gaspar, A. B.; Ksenofontov, V.; Seredyuk, M.; Gütlich, P. *Coord. Chem. Rev.* **2005**, *249*, 2661.
(4) Krivokapic, I.; Zerara, M.; Daku, M. L.; Vargas, A.; Enachescu, C.; Ambrus, C.; Tregenna-Piggott, P.; Amstutz, N.; Krausz, E.; Hauser, A. *Coord. Chem. Rev.* **2007**, *251*, 364. Gaspar, A. B.; Seredyuk, M.; Gütlich, P. *Coord. Chem. Rev.* **2009**, *253*, 2399. Gütlich, P.; Gaspar, A. B.; Garcia, Y. *Beilstein J. Org. Chem.* **2013**, *9*, 342.
(5) Kahn, O.; Martinez, C. J. *Science* **1998**, *279*, 44.
(6) Oshio, H.; Kitazaki, K.; Mishiro, J.; Kato, N.; Maeda, Y.; Takashima, Y. *J. Chem. Soc., Dalton Trans.* **1987**, 1341.
(7) Hayami, S.; Gu, Z.-Z.; Yoshiki, H.; Fujishima, A.; Sato, O. *J. Am. Chem. Soc.* **2001**, *123*, 11644.
(8) Hayami, S.; Kawahara, T.; Juhasz, G.; Kawamura, K.; Uehashi, K.; Sato, O.; Maeda, Y. *J. Radioanal. Nucl. Chem.* **2003**, *255*, 443.
(9) Spiering, H.; Meissner, E.; Köppen, H.; Müller, E. W.; Gütlich, P. *Chem. Phys.* **1982**, *68*, 65.
(10) Spiering, H. *Top. Curr. Chem.* **2004**, *235*, 171.
(11) Spiering, H.; Boukheddaden, K.; Linares, J.; Varret, F. *Phys. Rev. B* **2004**, *70*, 184.
(12) Wajnflasz, J.; Pick, R. *J. Phys. (Paris), Colloq.* **1971**, *32*, C1−91.
(13) Bousseksou, A.; Nasser, J.; Linares, J.; Boukheddaden, K.; Varret, F. *J. Phys. I (France)* **1992**, *2*, 1381.
(14) Bousseksou, A.; Varret, F.; Nasser, J. *J. Phys. I* **1993**, *3*, 1463.
(15) Bousseksou, A.; Constant-Machado, J.; Varret, F. *J. Phys. I* **1995**, *5*, 747.
(16) Boukheddaden, K.; Shteto, I.; Hôo, B.; Varret, F. *Phys. Rev. B* **2000**, *62*, 14796 ; 62,14806.
(17) Nishino, M.; Miyashita, S.; Boukheddaden, K. *J. Chem. Phys.* **2003**, *118*, 4594.
(18) Nishino, M.; Boukheddaden, K.; Miyashita, S.; Varret, F. *Phys. Rev. B* **2005**, *72*, 064452.
(19) Miyashita, S.; Konishi, Y.; Tokoro, H.; Nishino, M.; Boukheddaden, K.; Varret, F. *Prog. Theor. Phys.* **2005**, *114*, 719.
(20) Kambara, T. *J. Phys. Soc. Jpn.* **1980**, *49*, 1806.
(21) Sasaki, N.; Kambara, T. *J. Chem. Phys.* **1981**, *74*, 3472.
(22) Sasaki, N.; Kambara, T. *Phys .Rev. B* **1989**, *40*, 2442.
(23) Klokishner, S. I.; Varret, F.; Linares, J. *Chem. Phys.* **2000**, *255*, 317.
(24) Klokishner, S. I.; Linares, J. *Phys. Chem. C* **2007**, *111*, 10644.
(25) Klokishner, S. I.; Linares, J.; Varret, F. *J. Phys.: Condens. Matter* **2001**, *13*, 595.
(26) Klokishner, S. I. *Chem. Phys.* **2001**, *269*, 411.
(27) Klokishner, S.; Roman, M.; Reu, O. *Inorg. Chem.* **2011**, *50*, 11394.
(28) Klokishner, S.; Ostrovsky, S.; Palii, A.; Shatruk, M.; Funck, K.; Dunbar, K. R.; Tsukerblat, B. *J. Phys. Chem. C* **2011**, *115*, 21666.
(29) Ostrovsky, S.; Palii, A.; Klokishner, S.; Shatruk, M.; Funck, K.; Achim, C.; Dunbar, K. R.; Tsukerblat, B. In *Vibronic Interactions and the Jahn−Teller Effect: Theory and Applications, Progress in Theoretical Chemistry and Physics*; Atanasov, M., Tregenna, P. , Daul, C., Eds.:, Springer: New York, 2012, *23*, 379.
(30) Roman, M.; Reu, O.; Klokishner, S. *J. Phys. Chem. A* **2012**, *116*, 9534.
(31) Clemente-Leon, M.; Coronado, E.; Gimenez-Lopez, M. C.; Soriano-Portillo, A.; Waerenborgh, J. C.; Delgado, F. S.; Ruiz-Perez, C. *Inorg. Chem.* **2008**, *47*, 9111.
(32) Clemente-Leon, M.; Coronado, E.; Lopez-Jorda, M.; Minguez Espallargas, G.; Soriano-Portillo, A.; Waerenborgh, J. C. *Chem.—Eur. J.* **2010**, *16*, 2207.
(33) (a) Clemente-León, M.; Coronado, E.; López-Jordà, M. *Dalton Trans.* **2010**, *39*, 4903. (b) Clemente-León, M.; Coronado, E.; López-Jordà, M.; Waerenborgh, J. C. *Inorg. Chem.* **2011**, *50*, 9122. (c) Clemente-León, M.; Coronado, E.; López-Jordà, M. *Eur. J. Inorg. Chem.* **2013**, 753.
(34) Clemente-Leon, M.; Coronado, E.; Marti-Gastaldo, C.; Romero, F. M. *Chem. Soc. Rev.* **2011**, *40*, 473.
(35) (a) Clemente-León, M.; Coronado, E.; López-Jordà, M.; Desplanches, C.; Asthana, S.; Wang, H.; Létard, J.-F. *Chem. Sci.* **2011**, *2*, 1121. (b) Clemente-Leon, M.; Coronado, E.; Lopez-Jorda, M.; Waerenborgh, J. C.; Desplanches, C.; Wang, H.; Létard, J.-F.; Hauser, A.; Tissot, A. *J. Am. Chem. Soc.* **2013**, *135*, 8655.
(36) Sugano, S.; Tanabe, Y.; Kamimura, H. *Multiplets of Transition-Metal Ions in Crystals*; Academic Press: New York, 1970.
(37) Biernach, S. W.; Kaminska, A.; Suchocki, A.; Arizmendi, L. *Appl. Phys. Lett.* **2002**, *81*, 442.
(38) Vasiliev, A. V.; Malkin, B. Z. *Sov. Solid State Phys.* **1975**, *17*, 3167.

(39) Malkin, B. Z. Crystal field and electron-phonon interaction in rare-earth ionic paramagnets. In *Spectroscopy of Solids Containing Rare-Earth Ions*; Kaplyanskii, A.A., Macfarlane, R.M., Eds.; North-Holland: Amsterdam, 1987; p13.
(40) Popova, M. N.; Chukalina, E. P.; Malkin, B. Z.; Saikin, S. K. *Phys. Rev. B* **2000**, *61*, 7421.
(41) Klokishner, S.; Melsheimer, J.; Jentoft, F. C.; Schlögl, R. *Phys. Chem. Chem. Phys.* **2004**, *6*, 2066.
(42) Klokishner, S. I.; Tsukerblat, B. S.; Reu, O. S.; Palii, A. V.; Ostrovsky, S. M. *Chem. Phys.* **2005**, *316*, 83.
(43) Klokishner, S. I.; Tsukerblat, B. S.; Reu, O. S.; Palii, A. V.; Ostrovsky, S. M. *Opt. Mater.* **2005**, *27*, 1445.
(44) Klokishner, S. I.; Reu, O. S.; Ostrovsky, S. M.; Palii, A. V.; Kulyuk, L. L.; Tsukerblat, B. S.; Towe, E. *J. Mol. Struct.* **2007**, *838*, 133.
(45) Klokishner, S.; Reu, O.; Ostrovsky, S.; Palii, A.; Towe, E. *J. Phys.: Condens. Matter* **2007**, *19*, 486213.
(46) Klokishner, S. I.; Reu, O.; Chan-Thaw, C. E.; Jentoft, F. C.; Schlögl, R. *J. Phys. Chem.* **2011**, *A 115*, 8100.
(47) Klokishner, S.; Behrens, M.; Reu, O.; Tzolova-Möuller, G.; Girgsdies, F.; Trunschke, A.; Schlögl, R. *J. Phys. Chem.* **2011**, *A 115*, 9954.
(48) Clementi, E.; Roetti, C. *At. Data Nucl. Data Tables* **1974**, *14*, 177.
(49) Abragam, A.; Bleaney, B. *Electron Paramagnetic Resonance of Transition Ions*; Clarendon Press: Oxford, U.K., 1970.
(50) Gehring, G. A.; Gehring, K. A. *Rep. Prog. Phys.* **1975**, *38*, 1.
(51) Decurtins, S.; Gütlich, P.; Köhler, C. P.; Spiering, H.; Hauser, A. *Chem. Phys. Lett.* **1984**, *105*, 1.
(52) Hayami, S.; Hiki, K.; Kawahara, T.; Maeda, Y.; Urakami, D.; Inoue, K.; Ohama, M.; Kawata, S.; Sato, O. *Chem.—Eur. J.* **2009**, *15*, 3497−3508.